Volume 13, Number 2, 2020. pp. 137-147

Jordan Journal of Physics

ARTICLE

Theoretical Simulation of Backscattering Electron Coefficient for Si_xGe_{1-x}/Si Heterostructure as a Function of Primary Electron Beam Energy and Ge Concentration

A.M.D. Assa'd and **H. Kawariq**

Department of Basic Sciences, Faculty of Arts and Sciences, Al-Ahliyya Amman University, Amman 19328, Jordan.

Doi : https://doi.org/10.47011/13.2.5

Received on: 29/09/2019; *Accepted on: 16/2/2020*

Abstract: This study aims to investigate the backscattering electron coefficient for Si_xGe_{1-x}/Si heterostructure sample as a function of primary electron beam energy (0.25-20 keV) and Ge concentration in the alloy. The results obtained have several characteristics that are as follows: the first one is that the intensity of the backscattered signal above the alloy is mainly related to the average atomic number of the Si_xGe_{1-x} alloy. The second feature is that the backscattering electron coefficient line scan shows a constant value above each layer at low primary electron energies below 5 keV. However, at 5 keV and above, a peak and a dip appeared on the line scan above Si-Ge alloy and Si, respectively, close to the interfacing line. Furthermore, the shape and height of peak and dip broadening depend on the primary electron energy and incidence position with respect to the interfacing line. The last feature is that the spatial resolution of the backscattered signal at the interfacing line is improving by decreasing the primary electron energy (below 5 keV) and the shared element (Si) concentration. On the other hand, a poor compositional contrast has been shown at low primary electron energy below 5 keV. For energies above 5 keV, the spatial resolution becomes weak. These results can be explained by the behavior of the incident electrons inside the solid (interaction volume), especially at a distance close to the interfacing line and their chance to backscatter out of the sample. In general, a good compositional contrast with a high spatial resolution can be achieved at primary electron energy equal to 1 keV.

Keywords: Monte Carlo model, Backscattering electron coefficient, Si-Ge/Si, Elastic scattering, Spatial resolution, Compositional contrast.

Introduction

The development on the field emission source in getting a small probe size at low electron energies in SEM has improved the spatial resolution in the topographic contrast and reduced the charging and radiation damage of biological and semiconductor samples [1-5]. Using SEM for nano-scale sample imaging becomes recently one of the most important challenges [1, 6]. The images on SEM are produced by collecting either the backscattered electrons (BSEs) or secondary electrons (SEs). The image contrast in SEM is normally related to backscattering electron coefficient (η) and secondary electron yield (δ) which are functions of the target atomic number (Z), incident electron beam energy (E_p) and angle of incidence (θ). Conventionally, secondary electron yield (δ) is defined as the ratio of the number of the electrons escaping with energies below 50 eV to the number of the primary electrons. These secondary electrons are mainly generated as a

Corresponding Author: A.M.D. Assa'd **Email**: ajaber@ammanu.edu.jo

result of inelastic scattering between the primary electrons and the outer shell electrons of the target atoms. The collected secondary electrons are those electrons that escaped from the few nanometers depth beneath the surface [1, 2]. The backscattering electron coefficient (η) is defined as the ratio of the number of electrons that exit the surface with energy greater than 50 eV to the number of primary electrons impinging on the surface. The choice of the 50 eV value is purely arbitrary and historical. The secondary electrons with energy higher than 50 eV are produced as a result of electron beam–solid interaction. The number of these secondary electrons is rather small in comparison with the backscattered electrons and can be safely neglected [7]. BSE signals are normally used for the compositional contrast and elemental distribution, while SE signals are used for topographical contrast [1, 2]. Several experimental works have been conducted in order to provide accurate data for η and δ [7-14].

This paper presents the results of the Monte Carlo simulation of the backscattering electron coefficient for Si_xGe_{1-x}/Si heterostructure as a function of primary electron beam energy (0.25-20 keV) and Ge concentration using CASINO model [15]. The counted backscattered electrons are those primary electrons that escaped from the surface with energy above 50 eV. Si-Ge alloys are widely used in semiconductor industry [16]. Si-Ge alloys with different fractions of Ge (1-x) are used in MOSFETs as stressors to introduce strain into Si and Ge channels. This is due to the lattice constant of Si-Ge alloys which is different from that of Si and Ge and is easily controlled by the fraction of Ge [17]. The mechanical strength of the alloy becomes temperature-insensitive at elevated temperatures depending on the alloy composition [18]. Understanding electron-solid interaction is important for surface analysis in many technological applications. For example, in Scanning Electron Microscopy (SEM), this can help significantly improve the image quality in terms of contrast and spatial resolution. When analyzing insulator targets, sample charging phenomenon can have adverse effects on the resulting image to a certain extent. Another point concerns the obtaining of a good contrast between different objects, which depends on such quantities as, for example, the incident energy of the electron beam and the attenuation coefficient in different parts of the investigated target [1, 2]. The right choice of different experimental parameters may significantly improve the resulting images. However, sometimes, there is no possibility to check all of them in one experiment (this can be time- and money-consuming). Therefore, the use of theoretical simulation can help predict the resulting image quality. One of the widely used approaches is the Monte Carlo simulation model which allows to take many different effects and parameters into account [19-25]. The result of such a simulation strongly depends on input parameters, such as electron scattering characteristics. The authors used the Mott elastic cross-sections to describe elastic scattering of electrons in solid which is indeed among the most reliable data [26]. The primary electron energy loss due to inelastic scattering has been calculated by applying the semi-empirical equation of Joy and Lui [27]. This equation is proved to be simple and accurate as it was applied in a wide range of primary electron energies, especially low electron energies. The primary electrons on one side of the target start penetrating and interacting with the target atoms until losing their energy (which becomes less than 50eV), backscatter from the surface to vacuum or penetrate the interfacing line toward the next layer of the target. The interfacing line is considered as a surface of the penetrated layer. Hence, the electrons penetrating the interfacing line keep scattering inside the new layer until they backscatter to the old layer, backscatter to the vacuum from the target surface as backscattered electrons or lose all of their energy (minimum $E_P = 50$ eV).

Results and Discussion

Fig. 1 shows the simulation geometry of the present theoretical study and the corresponding profile of the volume of electron-solid interaction. The interaction volume is the place where the incident electrons are scattered (elastic and inelastic) with the solid atoms. Fig. 2 shows the interaction volume for Si and Ge layers at E_p = 5, 10 and 20 keV. It is clear that the incident electrons penetrating a target are broadened from the incidence position. The size and shape of the interaction volume are depending on the primary electron energy (E_P) and the characteristic parameters of the target material (average atomic number (Z_{avr}), atomic mass number (A) and density (ρ)) [1, 2, 28]. Generally, the interaction volume inside the Ge layer is smaller than that in the Si layer, since the

atomic number of Ge is larger than that of Si. Thus, the incident electrons have a small range inside the Ge layer. This keeps them interacting with the Ge atoms close to the layer surface and gives the incident electrons a chance to backscatter to vacuum with a small loss of their primary energy. In the case of Si layer, the incident electrons will penetrate deeper and spread wider than those electrons that penetrate the Ge layer. The incident electrons will also suffer a large amount of energy loss inside the Si layer more than inside the Ge layer. Fig. 2 shows that as the incident electron energy increases, the interaction volume depth (R) and radius (r) increase [29]. Generally, the interaction volume of the incident electrons in the Si-Ge alloy with different Ge concentrations is smaller than in the pure Si side for the entire E_P range. This is due to that Z_{avr} of the Si-Ge alloy is larger than that of the Si layer. Therefore, the incident electrons in the alloy have a larger chance to reach the surface and be backscattered to vacuum after penetrating and scattering with the alloy atoms than those incident on the pure Si side.

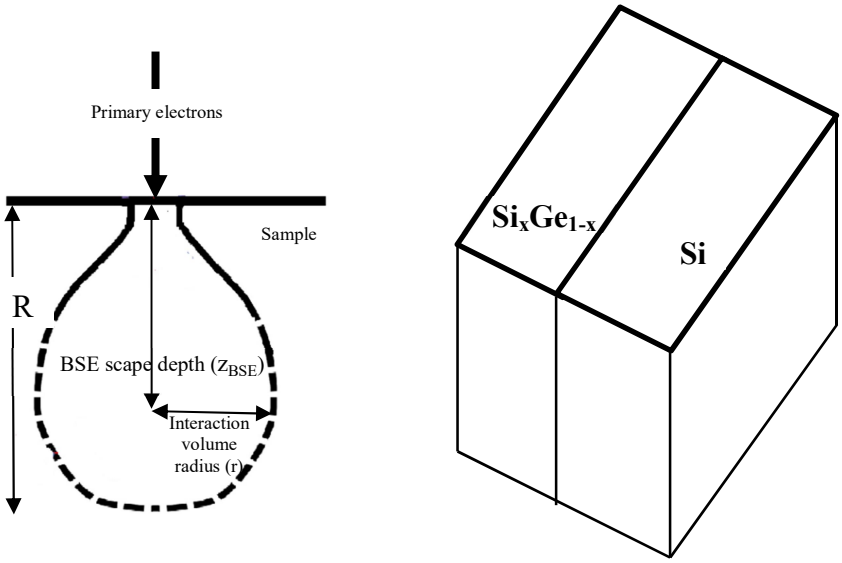

FIG. 1. Schematic diagram of the interaction volume of electron-solid interaction showing the BSE escape depth (z_{BSE}) and the interaction volume radius (r).

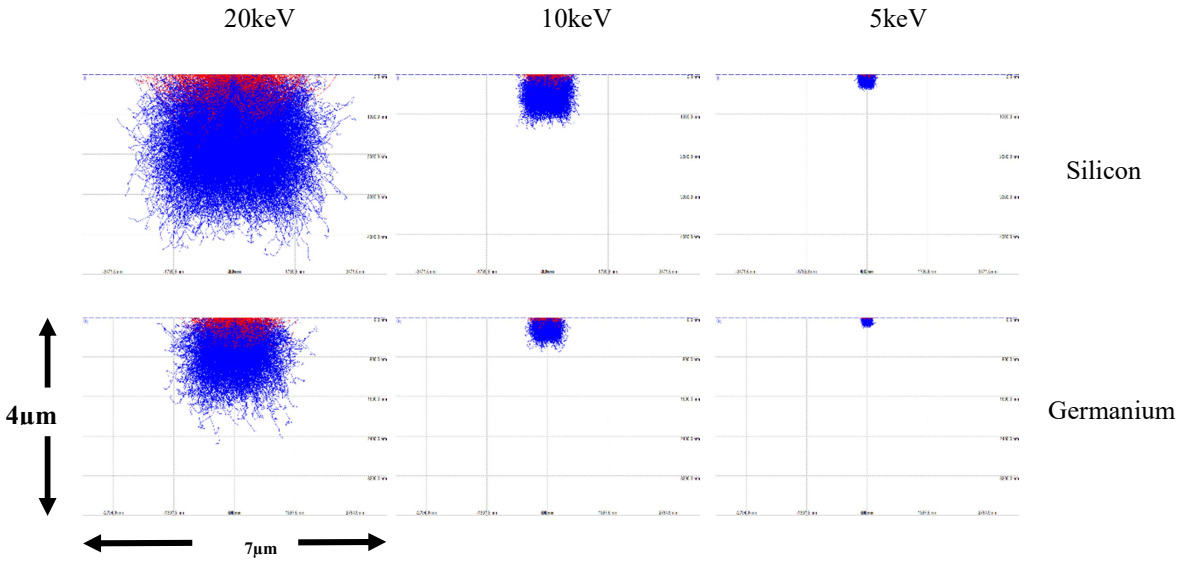

FIG. 2. Monte Carlo simulations of electron-solid interaction for Si and Ge at E_P = 5 keV, 10 keV and 20 keV.

In the case of micro-scale dimensions where the sample structure width is above 400 nm, η line scan has been calculated for different Ge concentrations as a function of E_P, as shown in Fig. 3. Fig. 4 also shows η line scan of different E_P values as a function of Ge concentration on Si_xGe_{1-x} alloy. The results show that the signal intensity above the alloy is higher than that above the Si side. The results also show that η above the Si-Ge alloy depends on the Ge concentration [30]. This is mainly because Z_{avr} is increasing as the Ge concentration increases. A peak above the alloy side and a dip above the pure Si side have been shown in the line scan around the interfacing line at primary electron energies of 5 keV and above; Fig. 4 (c, b, e). The position, height and sharpness of the peak and the width of the dip are directly depending on Z_{avr} of the alloy, E_P and the beam incidence position from the interfacing line. These artefacts have been also observed in separate studies [31, 32], where the edge effect on η and the backscattered Auger signals have been investigated. The dip in the signal was explained due to the edge shadowing effect, whereas the peak was due to the increase in the escape probability of the incident electron from the edge side. Hence, the artefacts shown in the present results could be explained by studying the behavior of the incident electrons inside the sample close to the interfacing line.

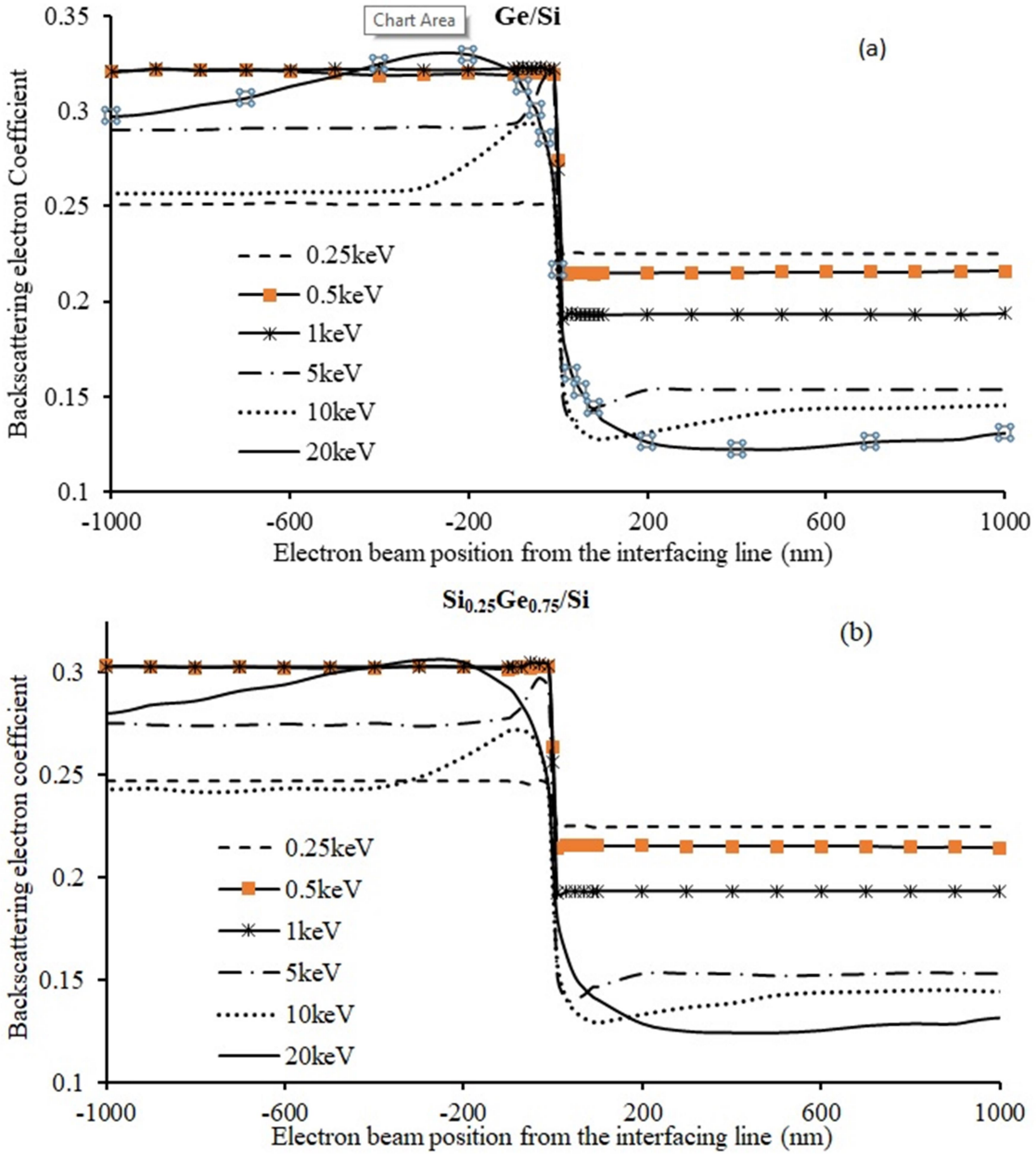

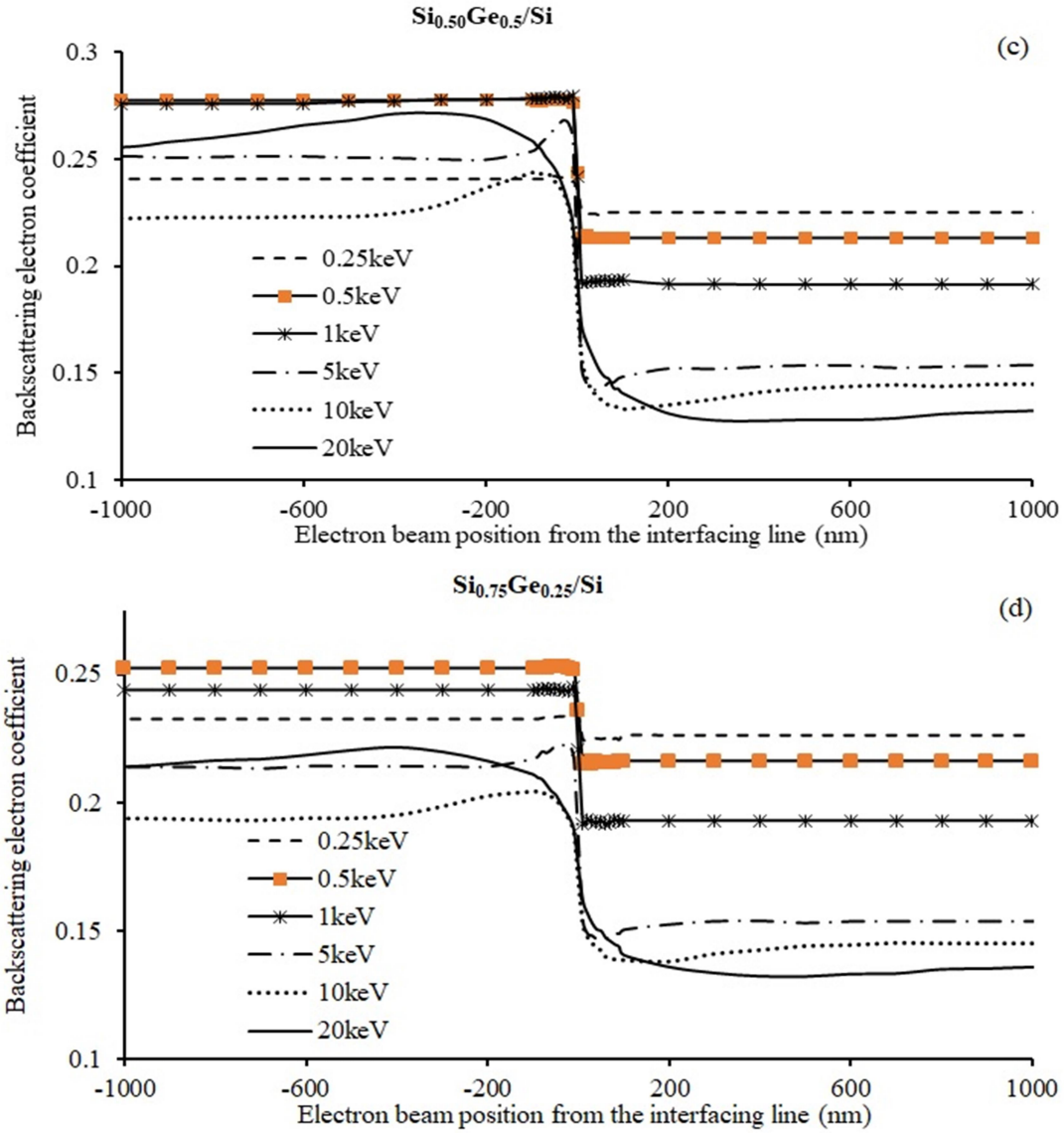

FIG. 3. Backscattering electron coefficient line scan as a function of primary electron energy for different x concentrations of Si_xGe_{1-x}/Si alloy.

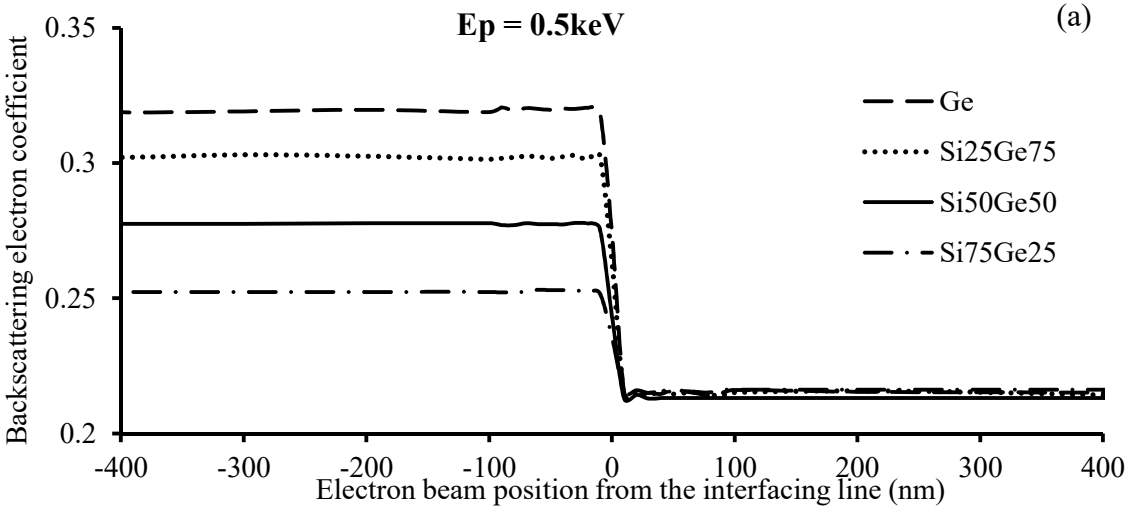

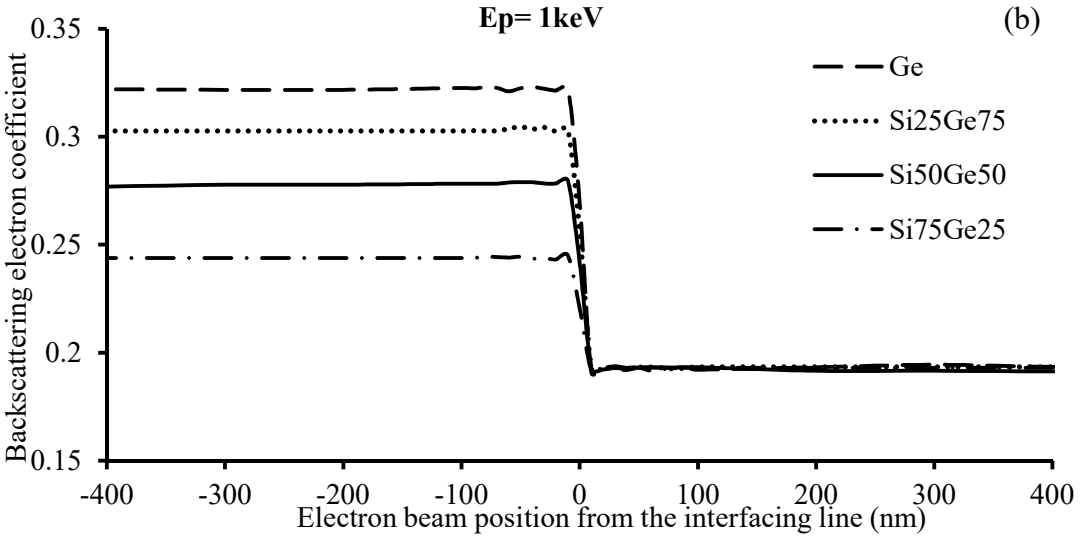
Ep= 1keV
(b)
Ge
Si25Ge75
Si50Ge50
Si75Ge25
Backscattering electron coefficient
0.35
0.3
0.25
0.2
0.15
-400 -300 -200 -100 0 100 200 300 400
Electron beam position from the interfacing line (nm)

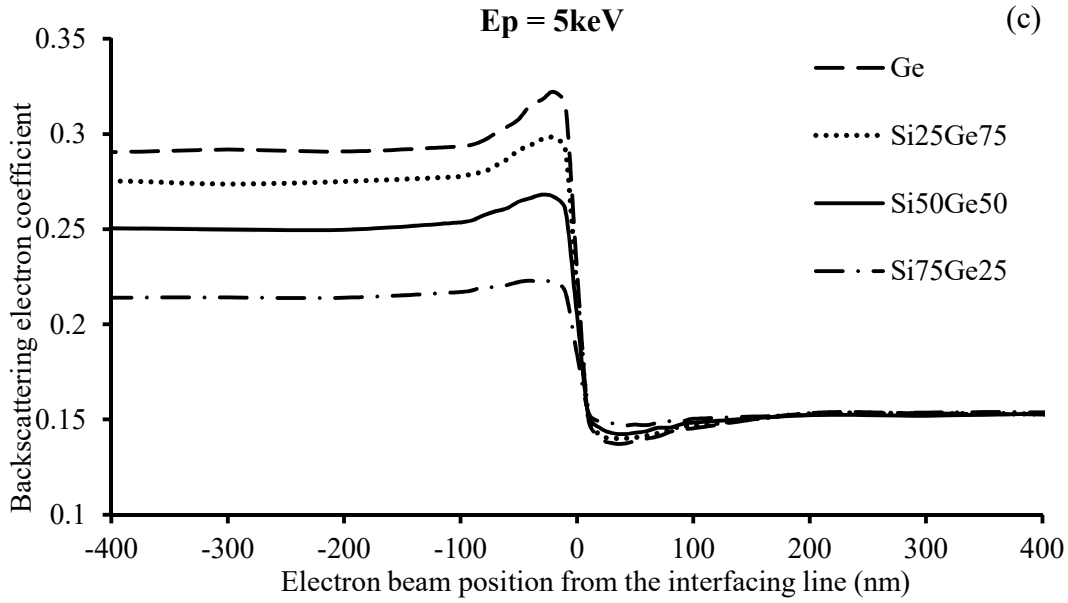
Ep = 5keV
(c)
Ge
Si25Ge75
Si50Ge50
Si75Ge25
Backscattering electron coefficient
0.35
0.3
0.25
0.2
0.15
0.1
-400 -300 -200 -100 0 100 200 300 400
Electron beam position from the interfacing line (nm)

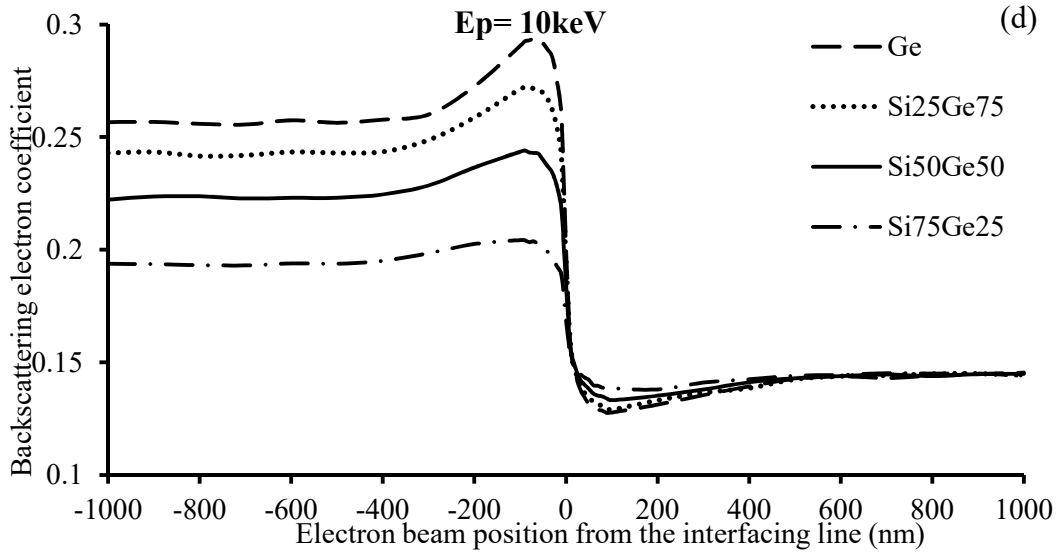
Ep= 10keV
(d)
Ge
Si25Ge75
Si50Ge50
Si75Ge25
Backscattering electron coefficient
0.3
0.25
0.2
0.15
0.1
-1000 -800 -600 -400 -200 0 200 400 600 800 1000
Electron beam position from the interfacing line (nm)

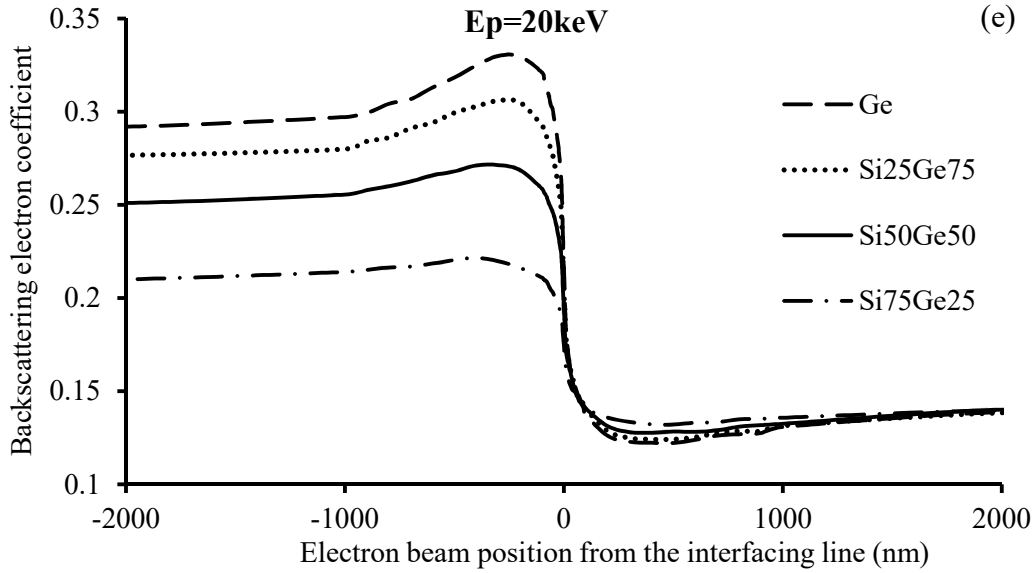

FIG. 4. Backscattering electron coefficient line scan as a function of x concentration of Si_xG_{1-x}/Si at different primary electron energies (E_P = 0.5-20 keV).

For $E_P \leq 1$ keV, the backscattering electron coefficient (η) line scan with a sharp step above the interfacing line can be observed for all Ge concentrations; Fig. 4 (a, b). This gives an indication that η data is reflected only from the primary electrons incident on the sample. This means that the interaction volume did not spread away from the incidence position. The latter is reflected on having a good spatial resolution for all x concentrations of Si_xGe_{1-x} alloy at low E_P. On the contrary, a compositional contrast between the Si-Ge alloy and Si reduces as E_P decreases (at E_P = 0.25keV) and the Ge concentration decreases; Fig. 3. This is because η values for the alloy and the Si layer become close to each other. In other words, the material contrast is no more proportional to the atomic number at primary electron energies below 0.5 keV [1, 7, 13]. As E_P increases above 1 keV, the compositional contrast improved while the spatial resolution reduced; Fig. 4 (c, d, e). This is due to the appearance of the peak above the Si-Ge alloy and the dip above the Si side. Also, the spatial resolution decreases as E_P increases and the Ge concentration decreases in the alloy. This appears in the increment in the distance between the peak and the dip. The reasons of having a peak and a dip above the Si-Ge alloy and Si, respectively, could be explained through the backscattered electron escape depth (z_{BSE}) and the interaction volume radius (r) of the primary electrons in the solid. When the primary electrons impinge on the Si-Ge alloy side at a distance from the interfacing line smaller than the radius (r) of the interaction volume, many of these electrons will reach the Si layer through the interfacing line. And because of their small depth which is close to the surface and the sufficient energy in addition to their large mean free path length in the Si layer, these electrons could find their way to the vacuum through the Si surface. As E_P increases and Ge concentration decreases, the peak height decreases and becomes wider and shifting way from the interfacing line; Fig. 4. The reduction in η values is due to the reduction in the average atomic number (Z_{avr}) of the Si-Ge alloy as a result of the reduction in Ge concentration. The broadening in the peak is due to the increase in the mean free path length of the primary electrons in the alloy, which reflects on the increase of z_{BSE} and r. Hence, the interaction volume will cover part of the Si layer while the primary electrons are incident on the Si-Ge alloy at a long distance from the interfacing line. This means that as the Ge concentration deceases and E_P increases, more primary electrons can find their way to the vacuum through the Si side. The results also show that the peak appears on the line scan when the ratio of the incident position from the interfacing line to the interaction volume radius (r) is around 70% for all Ge concentrations and E_P.

In the case where primary electrons are incident on the Si side, a dip in the backscattering electron line scan is observed; Figs. 3 and 4. This is clear when the distance between the incidence position and the interfacing line is less than the interaction volume radius (r). This is due to the large depth of the interaction volume from the surface. When some electrons pass the interfacing line toward the Si-Ge alloy, they stay and interact with the alloy materials at a large depth from the alloy surface. Because of the small mean free path length of primary electrons inside the Si-Ge alloy, these electrons will not backscatter to the vacuum from this large depth where they entered the alloy from the Si side. Even though some of these primary electrons could be scattered back toward the Si side, this would occur with no enough energy that allows them to reach the surface. So, the Si-Ge alloy prevents the primary electrons that entered the alloy from reaching the surface and being backscattered to the vacuum. As E_P and Ge concentration increase, the dip width increases and becomes deeper; Fig. 4. This is due to the large escape depth of the primary electrons in the Si side, as explained above.

Fig. 5 shows the backscattering electron coefficient (η) line scan for Si_xGe_{1-x}/Si with different x concentrations and E_P values at nano-scale dimensions (± 100 nm around the interfacing line). It is clear that there are several features that can be observed. At E_P = 0.5 and 1keV, the compositional contrast between the two sides of the sample around the interfacing line is clear. However, at E_P = 5 keV, a wide peak appears above the alloy. At E_P = 10 keV and 20 keV, the compositional contrast becomes weaker, since the backscattering coefficient (η) increases above the alloy as the incidence position of the primary electron moves away from the interfacing line, while it decreases above the Si side. This shows that at E_P = 0.5 keV and 1 keV, a good spatial resolution and a compositional contrast can be obtained for all Ge concentrations in Si-Ge alloy.

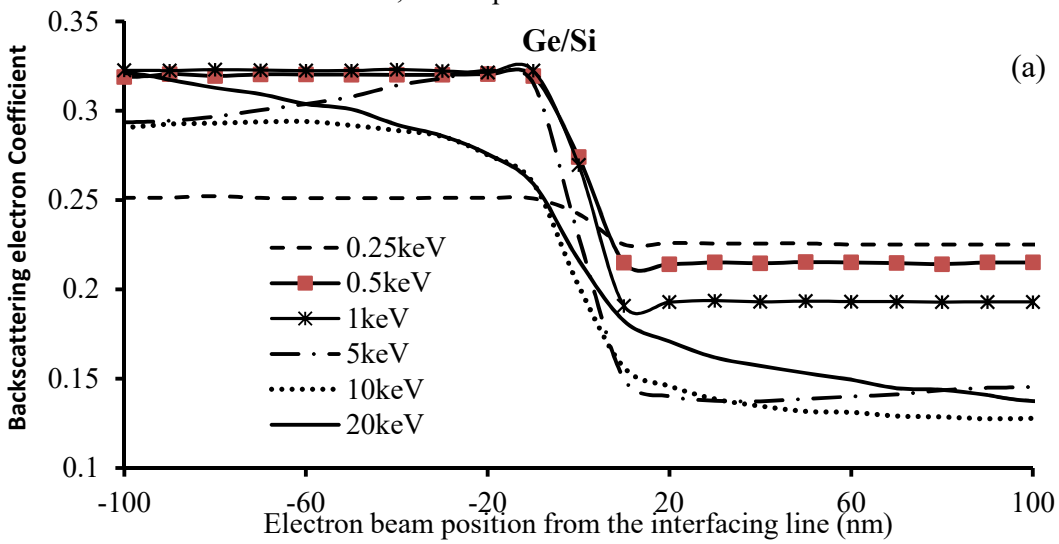

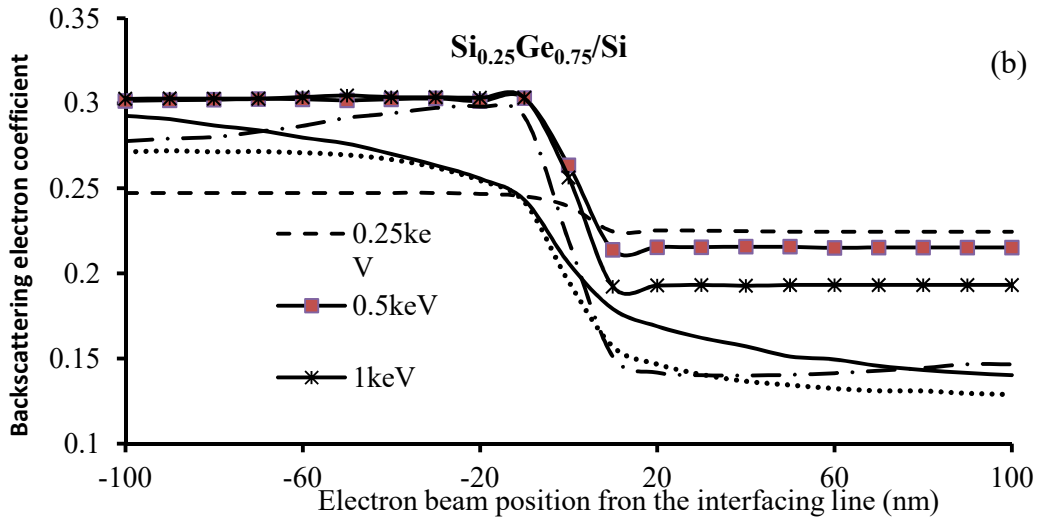

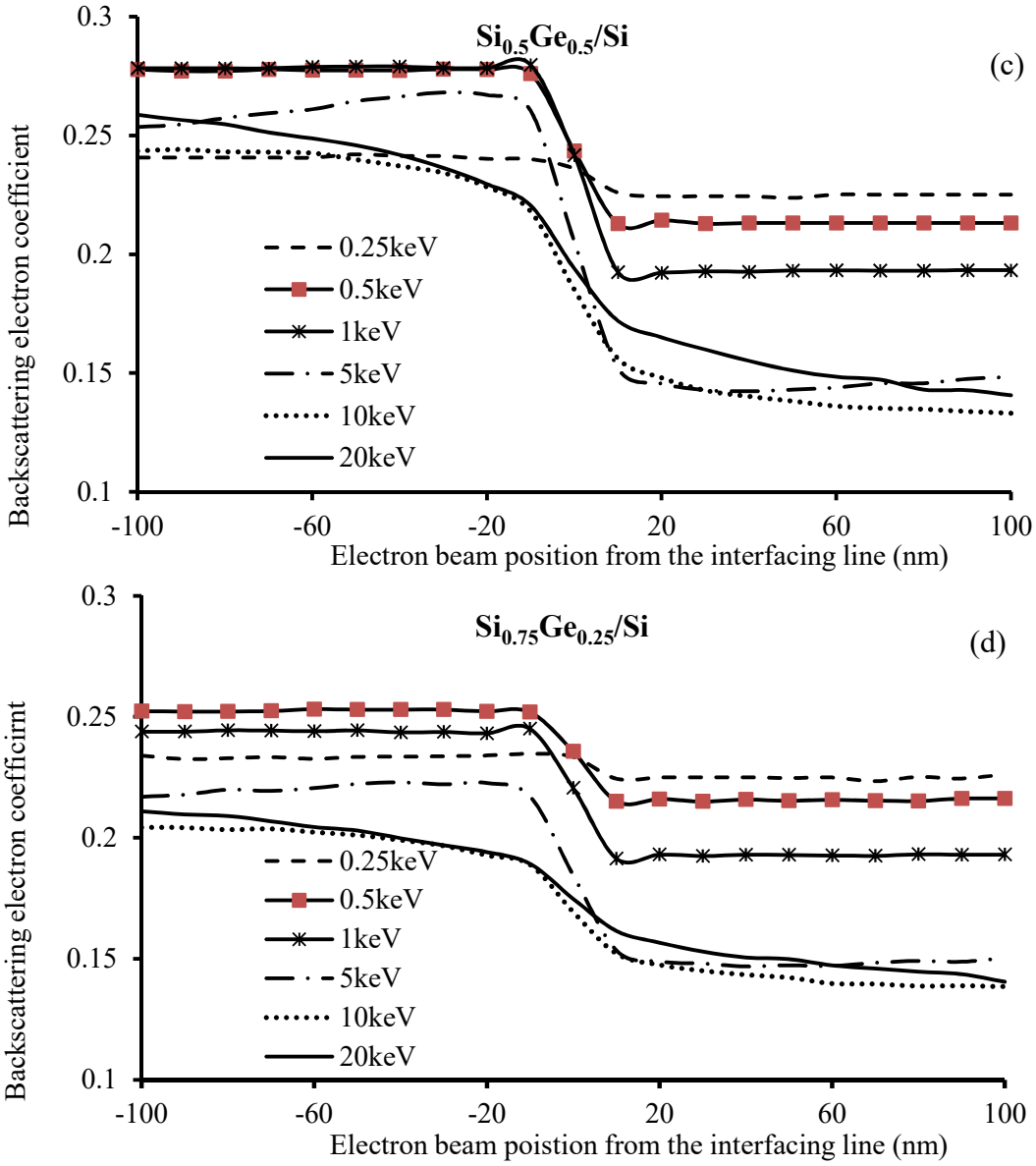

FIG. 5. Backscattering electron coefficient line scan as a function of primary electron energy for different x concentrations of Si_xGe_{1-x}/Si alloy at nano-scale dimensions (±100nm width around the interfacing line).

Conclusion

The Monte Carlo model is used in the present study in order to provide a better understanding of the artefacts shown in the backscattered electron signals obtained as a result of the interaction between the primary electrons and Si_xGe_{1-x}/Si heterostructure sample with different x concentrations and primary electron energies. The results show the effect of Ge concentration of the alloy and that of the primary electron energy on the compositional and spatial resolution of the backscattered signal. A good compositional contrast and spatial resolution in SEM imaging could be obtained at low primary electron energies of 0.5 keV and 1 keV. At higher primary electron energies (above 1 keV), a peak and a dip have been shown in the backscattering electron coefficient, which affected the spatial resolution and the compositional contrast.

Acknowledgement

This work was supported by Al-Ahliyya Amman University Project No. 1/20/2018-2019.

References

[1] Reimer, L., "Scanning Electron Microscopy, Physics of Image Formation and Microanalysis". (Springer, Berlin, Germany 1985).

[2] Goldstein, G.I., Newbury, D.E., Echlin, P., Joy, D.C., Fiori, C. and Lifshin, E., "Scanning Electron Microscopy and X-ray Microanalysis". (New York, Plenum Press, 1981).

[3] Jayakody, G.H., Wells, T.R.C. and El-Gomati, M.M., Journal of Electron Spectroscopy and Related Phenomena, 143 (2005) 2.

[4] El-Gomati, M.M., Zaggout, F., Jayacody, H., Tear, S. and Wilson, K., Surface and Interface Analysis, 37 (11) (2005) 901.

[5] Wuhrerm, R. and Moran, K., I.O.P Conf. Ser. Mater. Sci. Eng., 109 (2016) 1.

[6] Vida-Simit, I., Jumate, N., Chicinas, I. and Batin, G., Rom. Journ. Phys., 49 (9-10) (2004) 955.

[7] El-Gomati, M.M., Walker C.G.H., Assa'd, A.M.D. and Zadrazil, M., Scanning, 30 (2008) 2.

[8] Bronstein, I.M. and Fraiman, B.S. "Vtorichnaya Elektronnaya Emissiya", Secondary Electron Emission, (Nauka-Moskva, 1969).

[9] Assad, A.M.D. and El-Gomati, M.M., Scanning Microscopy, 12 (1998) 185.

[10] Joy, D.C. "A Database of electron solid interactions", Revision [04-02], (2006); http://web.utk.edu/~srcutk/htm/interact.htm].

[11] Walker, C.G.H., El-Gomati, M.M., Assa'd, A.M.D. and Zadražil, M., Scanning, 30 (2008) 365.

[12] Liu, S., Liu, Y., Wang, P., Liu, W., Pei, G., Zeng, L. and Sun, X., Review of Scientific Instruments, 89 (2018) 023303

[13] Hashimoto, Y., Muto, A., Woods, E., Walters, T. and Joy, D.C., Microscopy Today, May (2015) 20.

[14] Suria, A., Prattb, A., Tear, S., Walker, W., Kincal, C., Kamber, U., Gurlud, O. and El-Gomati, M., J. of Electron Spectroscopy and Related Phenomena (2019), in press, https://doi.org/10.1016/j.elspec.2019.02.002.

[15] Demers, H., Poirier-Demers, N., Couture, A.R., Joly, D., Guilmain, M., Jonge, N. and Drouin, D., Scanning, 33 (2011) 135.

[16] Mastronardi, L., Banakar, M., Khokhar, A.Z., Hattasan, N., Rutirawut, T., Domínguez, Bucio, T., Grabska, K.M., Littlejohns, C., Bazin, A., Mashanovich, G. and Gardes, F.Y., Optical Express, 26 (6) (2018) 6663.

[17] Takagi, S., "Silicon–Germanium (Si-Ge) Nanostructures (Production, Properties and Applications in Electronics)", (Woodhead Publishing Series in Electronic and Optical Materials, 2011), pp. 499–527.

[18] Yonenaga, I., "Six Ge_{1-x} Bulk Crystals, Encyclopedia of Materials: Science and Technology", 2nd Ed. (Elsevier, 2003) pp. 8647-8651.

[19] Bishop, H.E., Proc. Phys. Soc., 85 (1965) 855.

[20] Joy, D.C., Journal of Microscopy, 147 (1987) 51.

[21] Yan, H., El-Gomati, M.M., Prutton, M., Wilkinson, D.K., Chu, D.P. et al., Scanning, 20 (1998) 465.

[22] Salvat, F., Fernandez-Varea, J.M. and Sempau, J., In: PENELOPE-2006 Workshop Proceedings, Barcelona, Spain 4–7 July (2006).

[23] Drouin, D., Couture, A.R., Joly, D.C., Tastet, X., Vincent, A. and Gauvin, R.M. Scanning, 29 (2007) 92.

[24] Soref, R., IEEE J. Sel. Top. Quantum Electron., 12 (6) (2006) 1678.

[25] Gauvin, R., Lifshin, E., Demers, H., Horny, P. and Campbell, H., Microsc. Microanal., 12 (2006) 49.

[26] Mott, N.F. and Massey, H.S.W. "Theory of Atomic Collisions". (Oxford University Press, London, 1965).

[27] Joy, D.C. and Luo, S., Scanning, 11 (1989) 176.

[28] Lukiyanov, F.A., Rau, E.I. and Sennov, R.A., Bulletin of the Russian Academy of Sciences: Physics, 73 (4) (2009) 441.

[29] Müllerová, I., Frank, L., Mikmeková, Š. and Mikmeková, E.M., Microscopy and Microanalysis, 25 (S2) (2019) 472.

[30] Ajmal Khana, M., Algarnia, H., Bouarissac, N., Al-Hagana, O.A. and Alhuwaymeld, T.F., Ultramicroscopy, 195 (2018) 53.

[31] El-Gomati, M.M. and Assa'd, A.M.D., "Modern Developments and Applications in Microbeam Analysis", (Springer, Vienna, 1998), p. 333.

[32] Assa'd, A.M.D. and El-Gomati, M.M., Ultramicroscopy, 79 (1999) 1.